IEEE Access
Multidisciplinary ⋮ Rapid Review ⋮ Open Access Journal

Received 4 December 2023, accepted 24 December 2023, date of publication 28 December 2023,
date of current version 8 January 2024.

Digital Object Identifier 10.1109/ACCESS.2023.3347892

RESEARCH ARTICLE

Adaptive Enhancement Display of Chromatic Electrowetting Based on Color Conversion

MINGZHEN CHEN[1,2], SHANLING LIN[3], JIANPU LIN[3], ZHIXIAN LIN[1,2,3], AND TAILIANG GUO[1,2]
[1]School of Physics and Information Engineering, Fuzhou University, Fuzhou 350108, China
[2]National and Local United Engineering Laboratory of Flat Panel Display Technology, Fuzhou 350108, China
[3]School of Advanced Manufacturing, Fuzhou University, Quanzhou 362200, China

Corresponding author: Zhixian Lin (t98068@fzu.edu.cn)

This work was supported in part by the National Key Research and Development Program of China under Grant 2021YFB3600603, in part by the Natural Science Foundation of Fujian Province under Grant 2020J01468, and in part by the National Natural Science Foundation of China Youth Foundation under Grant 62101132.

ABSTRACT The charge capture of color inks in chromatic electrowetting electronic paper, the contact angle hysteresis and inconsistent aperture ratio result in a narrower color gamut and reduced contrast of the display screen. To address the issue, we propose an algorithm of the adaptive color conversion and the dynamic enhancement display based on the aperture ratio of the chromatic electrowetting. Firstly, the relationship between the aperture ratio of electrowetting and the increase or decrease of voltage was tested through an experimental platform. Then, combined with the change of the aperture ratio, the reasonable grayscale allocation is made for color space conversion. Furthermore, considering the average grayscales of each color, we design a method of the dynamic contrast enhancement and histogram equalization based on the segmentation of aperture ratios. In addition, in view of the problem of grayscale loss in the reflective display, we propose an adaptive algorithm of domain error diffusion with saturation enhancement to compensate for color loss. The experiments demonstrate that the images processed by our algorithm have shown certain improvements in evaluation indicators compared to images processed by other methods. Most significant of all, it has better visual display effect on chromatic electrowetting electronic paper, displaying more details.

INDEX TERMS Electrowetting on dielectric (EWOD), color conversion, image enhancement, image quality optimization.

I. INTRODUCTION

With the development of reflective display technology, the color gamut of displays has shifted from the RGB color gamut to the CMY color gamut. Compared to the electrophoretic display, the electrowetting display has faster response speed and richer colors. This makes it more likely to play dynamic videos on electronic paper displays. However, most of the image and video content is based on RGB color gamut. At the same time, there are currently factors such as contact angle hysteresis and charge capture on dielectric layer. These inevitably lead to issues such as narrow color gamut, low contrast, and unclear details. Therefore, it is particularly momentous to research the correlation of RGB gamut images on CMY gamut displays.

The associate editor coordinating the review of this manuscript and approving it for publication was Gangyi Jiang.

Regarding the color optimization, researchers generally optimized images from the perspectives of grayscale histogram equalization and gamma correction [1]. Combining color stretching, histogram equalization, amplitude compression, and saturation maximization methods, some researchers used correction gamma values to achieve grayscale enhancement [2], [3], [4]. Combining galaxy swarm optimization and particle swarm optimization, researchers used the method of weighted features and Gaussian distribution to achieve adaptive histogram equalization and gamma correction [3], [5], [6], [7].

On this basis, some researchers also segmented histograms through the mean and variance of grayscale components, as well as grayscale gradients. Each part grayscale was separately performed through methods such as neighborhood comparison, histogram equalization and gamma correction [8], [9], [10]. The image histogram was processed

by using power logarithmic transformation, and then the sub-histograms were segmented by adjusting the threshold. The sub-histograms were equalized with median to achieve image enhancement that maintains average brightness [9], [11].

Besides, some researchers adjusted the image foreground, background and color space in order to optimize the image quality [12], [13], [14]. Before researching the relationship between backlight and color, Pei et al. decomposed the image into multi-scale illumination and reflection layers to improve color saturation [15]. Yu et al. used color constancy and just-noticeable-difference (JND) transform in foreground and background brightness to optimize and enhance image contrast and color perception [16]. Through gamma correction and gamut adjustment in CIELAB color space, Azetsu et al. achieved chromaticity adjustment under the enhancement of brightness and tone enhancement [17].

Although these works have achieved good results, it is not considered that the effects of the different response speeds, ink movement rupture and reflux, charge capture of the hydrophobic layer, and contact angle hysteresis on the reflection display performance of electrowetting electronic paper. To make up for these shortcomings, we propose an adaptive method of dynamic enhanced display based on color conversion of chromatic electrowetting electronic paper. Specifically, we make the following three contributions: i) Combining the physical characteristics of chromatic electrowetting pixels, we propose a method of the color space conversion based on the allocation of the electrowetting aperture ratio to make the grayscale distribution of each color channel more reasonable; ii) After integrating the grayscale mean and the aperture ratio of different colors, we perform adaptive dynamic contrast enhancement and segmented histogram equalization based on the change rate of aperture ratio; iii) Based on the variation range of the aperture ratio and the different compression situations under each color electrowetting, each color channel adopts an adaptive algorithm of the domain error diffusion to compensate for the lack of grayscale.

II. METHOD

A. OVERALL PIPELINE

As the grayscale of the displayed image on electrowetting display is related to the aperture ratio of the electrowetting pixels, it is necessary to research the relationship between the driving voltage and the aperture ratio of the electrowetting pixels. We use a microscope with a high-speed camera to collect the moving pictures of the electrowetting driven by a function signal generator. Using the image cutting algorithm is to segment and calculate the aperture ratio of the electrowetting pixel [18]. For observing the variation of the aperture ratio with the driving voltage, we apply the voltages of the different ranges to the CMY monochrome displays through a function signal generator, respectively. Fig. 1 shows the variation of the aperture ratio of the CMY three-color electrowetting with the increase and decrease of the voltage, respectively, obtained from experimental testing. As the driving voltage of the CMY monochrome display increases to the opening voltage, it is not conducive to the grayscale segmentation of the image. Accordingly, we mainly use the method of high voltage drop to obtain more suitable grayscale display of the image.

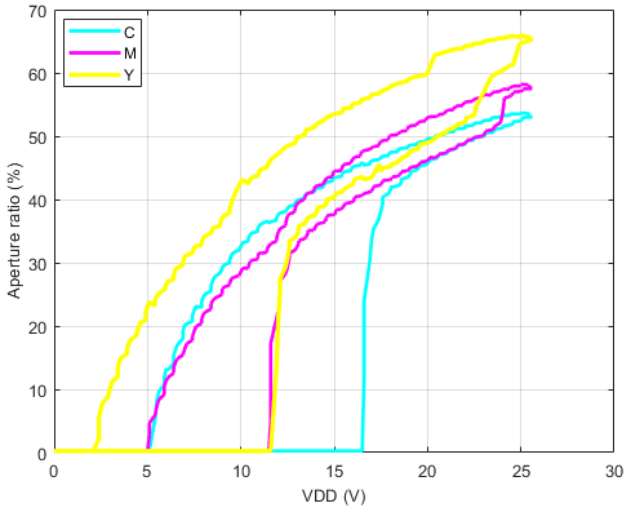

FIGURE 1. The changes in the aperture ratios of CMY electrowetting pixels within the driving voltage range.

When playing RGB images on the electrowetting of the CMY color gamut, we propose a method of adaptive color conversion and dynamic enhancement display based on the aperture ratio of electrowetting pixels, as shown in Fig. 2.

Because the maximum aperture ratio of CMY electrowetting cannot reach 100%, and the aperture rate of each color's electrowetting display is different. First of all, the sRGB image is subjected to RGB grayscale channel separation and normalization processing. Then, based on the maximum aperture ratio of electrowetting pixels, a method of adaptive gamma correction is proposed to convert into CIE 1931 XYZ color space through linear transformation. Next, the XYZ color coordinate values are normalized to convert into the LAB color space through the white reference point of the D65 light source. Ultimately, through the relationship between LAB and CMY color gamut, the color gamut conversion from LAB to CMY is achieved by linear conversion. To address the issues of color loss and contrast decrease after color conversion, we propose a dynamic enhancement method of error diffusion based on the maximum aperture ratio. Based on the average grayscale of each color channel and the maximum aperture ratio of the electrowetting, a method of adaptive exponential contrast enhancement is constructed. Furthermore, after transferring the color grayscale to the HSL color space, we achieve the adaptive saturation correction and enhancement under different brightness levels. At length, based on the different color compression situations of three-color electrowetting, the error after color compression is

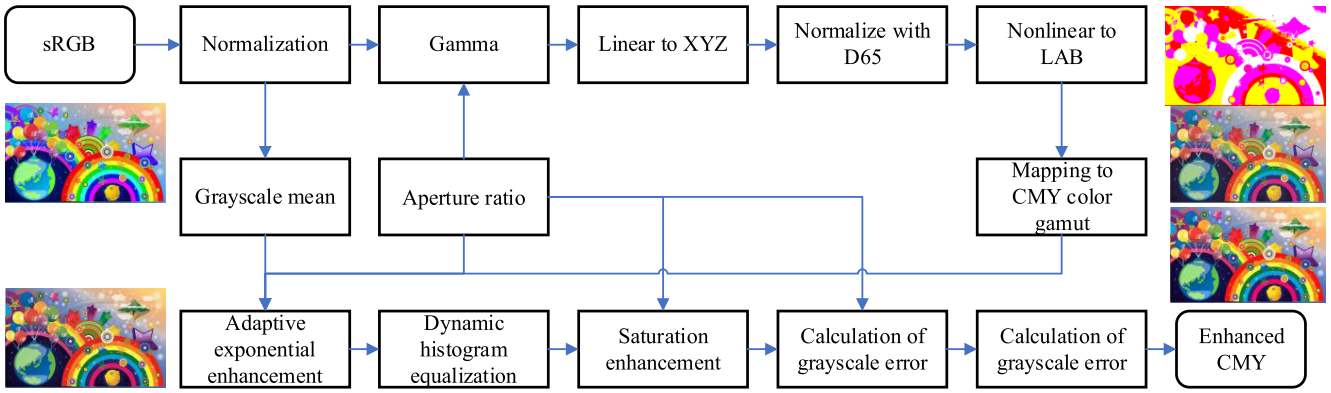

FIGURE 2. A method of adaptive color conversion and dynamic enhancement display based on the aperture ratio of electrowetting pixels.

calculated with pixel-by-pixel as the origin. Simultaneously, the error diffusion is carried out in the original pixel domain to compensate for the loss of color grayscale and enhance the contrast and saturation of the image.

B. COLOR CONVERSION

To address the issue of color space conversion for each color channel, we firstly separate the sRGB image into RGB channels, normalize the grayscale values of each color channel, and then perform adaptive gamma conversion to RGB images. Based on the different maximum aperture ranges of CMY electrowetting pixels, a gamma function for grayscale adaptation is constructed as follows:

$$\begin{cases} \mathrm{F(x,y)} = (I(\mathrm{x,y}))^{\gamma(x,y)} \\ \mathrm{g}(x,y) = 0.5^{(I(\mathrm{x,y})-\bar{I})/\bar{I}\cdot(100-A_{\max})/100} \end{cases} \tag{1}$$

where $\mathrm{F}(x,y)$ represents the corresponding grayscale values of the x,y pixel coordinates with the R, G, and B channels of the processed image, respectively; $\mathrm{I}(x,y)$ is the corresponding grayscale values in the R, G, and B channels of the original image; $\mathrm{g}(x,y)$ is the adaptive gamma correction values of each pixel point in R, G, and B channels, respectively; $\bar{I}$ is The average grayscale values of each channel R, G, and B, respectively; A_{max} is the maximum aperture ratio of the corresponding C, M, and Y color electrowetting pixels.

The grayscale values of the RGB three channels are linearly transformed into values in the CIE 1931 XYZ color gamut, and the linear transformation expression is

$$\begin{aligned} (\mathbf{X}\ \mathbf{Y}\ \mathbf{Z}) &= (\mathbf{R}\ \mathbf{G}\ \mathbf{B})\, M^{T}_{\mathrm{RGB2XYZ}} \\ &= (\mathbf{R}\ \mathbf{G}\ \mathbf{B}) \begin{pmatrix} 0.412453 & 0.357580 & 0.180423 \\ 0.212671 & 0.715160 & 0.072169 \\ 0.019334 & 0.119193 & 0.950227 \end{pmatrix}^{T} \end{aligned} \tag{2}$$

The XYZ color gamut values are normalized through the white reference points of the D65 light source, namely

$$\begin{cases} \mathbf{X_1} = \mathbf{X}/X_{ref\_white} \\ \mathbf{Y_1} = \mathbf{Y}/Y_{ref\_white} \\ \mathbf{Z_1} = \mathbf{Z}/Z_{ref\_white} \end{cases} \tag{3}$$

Then the normalized XYZ color gamut values is performed a nonlinear transformation, namely

$$\begin{aligned} &(\mathbf{X_2}, \mathbf{Y}_2, \mathbf{Z_2}) \\ &= \begin{cases} (\mathbf{X}_1, \mathbf{Y_1}, \mathbf{Z_1})^{1/3}, & (\mathbf{X}_1, \mathbf{Y_{11}}, \mathbf{Z_1}) \geq (6/26)^3 \\ (29/6)^2 \cdot (\mathbf{X}_1, \mathbf{Y_{11}}, \mathbf{Z_1})/3 + 16/116, & \text{else} \end{cases} \end{aligned} \tag{4}$$

$\mathbf{X_2}, \mathbf{Y_2}, \mathbf{Z_2}$ are perform a linear transformation to obtain the coordinate values of the Lab color space, namely

$$\begin{cases} \mathbf{L} = 116 \cdot Y_2 - 16 \\ \mathbf{a} = 500 \cdot (X_2 - Y_2) \\ \mathbf{b} = 200 \cdot (Y_2 - Z_2) \end{cases} \tag{5}$$

In the light of the color relationship between CMY and RGB, the coordinate values of the Lab color space are linearly mapped to the grayscale values of the CMY color gamut to obtain the RGB display of the image in the CMY color gamut. The linear conversion expression is

$$\begin{aligned} &(\mathbf{C}\ \mathbf{M}\ \mathbf{Y}) \\ &= (\mathbf{L}\ \mathbf{a}\ \mathbf{b})\, M^{T}_{\mathrm{Lab2CMY}} \\ &= (\mathbf{L}\ \mathbf{a}\ \mathbf{b}) \begin{pmatrix} -26.01074 & 195.50537 & -846.515805 \\ 2.863945 & 43.12107 & 70.45424 \\ 1.24269 & 19.83755 & 4.424395 \end{pmatrix}^{T} \end{aligned} \tag{6}$$

C. COLOR CONVERSION

An adaptive histogram equalization method of the dynamic threshold is proposed to address the issues of contrast reduction and detail loss caused by narrowing form RGB to CMY color gamut. Firstly, the grayscale channels are separated the grayscale RGB of the image in the CMY color gamut, and the

mean grayscales of each channel are calculated as the contrast threshold *th* of each channel. The reciprocal of the maximum aperture ratio A_{max} of each color electrowetting is used as the index for exponential contrast enhancement, namely

$$\mathrm{rgb} = 1/\left(1 + (\mathrm{th}/\mathrm{RGB})^{1/A_{\max}}\right) \times 255 \tag{7}$$

The variation curve of the aperture ratio with each color electrowetting are divided into three sections to perform segmented histogram equalization. Owing to the low saturation of the reflected display color on electrowetting electronic paper, we mapped the grayscale values to the HSL color space after histogram equalization. The overall brightness value L of the image is calculated on account of the grayscale value, and then the color saturation S is calculated in view of the brightness value L, namely

$$L = \left(\mathrm{rgb}_{\max} + \mathrm{rgb}_{\min}\right)/255/2 \tag{8}$$

$$S = \begin{cases} \left(\mathrm{rgb}_{\max} - \mathrm{rgb}_{\min}\right) / \left(\mathrm{rgb}_{\max} + \mathrm{rgb}_{\min}\right), \\ \qquad L < 0.5 \\ \left(\mathrm{rgb}_{\max} - \mathrm{rgb}_{\min}\right) / \left(512 - \mathrm{rgb}_{\max} - \mathrm{rgb}_{\min}\right), \\ \qquad L \geq 0.5 \end{cases} \tag{9}$$

where $\mathrm{rgb}_{\max}$ and $\mathrm{rgb}_{\min}$ are the maximum or minimum grayscale values in the CMY color gamut after color-channel separation. Based upon the maximum aperture ratio A_{max} of the CMY electrowetting, image grayscale after saturation enhancement rgb_1 is

$$\mathrm{rgb}_1 = \mathrm{rgb} + (\mathrm{rgb} - L \times 255) \times (A_{\max} - S) \tag{10}$$

Due to the limited grayscale displayed by the electrowetting display, the transmission method of the grayscale error field is improved to compensate for grayscale limitation based upon the different maximum aperture ratios. It further improves the grayscale similarity and signal-to-interference-noise ratio of the image on electrowetting display. After selecting a pixel as the origin, we obtain the error value by quantifying the grayscale level and rounding to zero. The error value is transferred to the surrounding 3 pixels. By analogy, the error transmission is carried out using pixel-by-pixel as the origin. The ultimate goal is to achieve image display using the grayscale compression and the error diffusion display on electrowetting electronic paper, compensating for the lack of color depth. The error transfer functions of its lower side, right and lower right are respectively represented as

$$\mathrm{rgb}_2' = \mathrm{rgb}_1 + \mathrm{rgb}_{\mathrm{er}} \times 3/8/A_{\max} \tag{11}$$

$$\mathrm{rgb}_2'' = \mathrm{rgb}_1 + \mathrm{rgb}_{\mathrm{er}}/4/A_{\max} \tag{12}$$

where rgb_2' is the error transfer value on the lower and right sides of the origin; rgb_1 is the RGB three-channel grayscale values of the original image before the error transmission; $\mathrm{rgb}_{\mathrm{er}}$ is the error value after the grayscale compression at the origin, and the sum of coefficients for three error diffusion points is 1; rgb_2'' 'is the error transfer value at the lower right of the origin.

III. EXPERIMENT

A. SUBJECTIVE EVALUATION

We processed all images in our image dataset, the Berkeley segmentation dataset: image dataset of 300 images and CBSD68 dataset [19], [20]. Different algorithms are used to compare the image effects before and after processing, such as Du et al. [21], Braik et al. [22], Xu et al. [23], and Hu et al. [24], as shown in Fig. 3. By comparing Fig. 3 (a) to Fig. 3 (f), it can be seen that the colors in Fig. 3 (b) and Fig. 3 (c) have been enhanced to a certain extent after gamut conversion; but the overall brightness has decreased, and the color contrast is not high enough in some cases. Fig. 3 (d) and Fig. 3 (e) have good color restoration after color gamut conversion, but the overall brightness of processed images is brighter, and some scenes have lower saturation and contrast. Due to the reflective display and narrower color gamut of the electrowetting display, images with lower or higher brightness will cause the display to be too dark or too bright. It is not conducive to the detailed display of the images. At the same time, a lower saturation of the image can also result in lighter colors and lower contrast on the electrowetting display. Fig. 3 (f) shows that the adaptive dynamic enhancement algorithm based on color space conversion in this paper takes into account both brightness and color to achieve color conversion and enhancement of images on electrowetting display. Through a certain degree of color shift and contrast-and-saturation enhancement, more image details are displayed on the electrowetting screen.

B. OBJECTIVE EVALUATION

Referring to the RGB original images, we calculate the objective evaluation indicators of grayscale similarity (GS), information entropy (IE), signal-to-noise ratio (SNR), and structural similarity (SSIM) of the images before and after processing by various algorithms. Table 1 shows the various objective evaluation indicators before and after all images in the datasets are processed by different methods. From the table, it can be seen that our algorithm has an image grayscale similarity of over 73%, an information entropy of over 7.8, a signal-to-noise ratio of over 7.9, and a structural similarity of over 83% in the CMY color gamut. By comparison, the average natural image quality evaluator (NIQE) of the original image is 4.0486. All the optimization methods have a certain improvement, among which our method has reached above 4.5. Overall, all image evaluation indicators are superior to other methods.

TABLE 1. Objective evaluation indicators for images processed by each method.

Method	GS	IE	SNR	SSIM	NIQE	Time (s)
Du et al.	0.6487	7.7601	7.5223	0.7331	4.115	130.56
Braik et a	0.6698	7.6892	7.6527	0.7602	4.2136	117.39
Xu et al.	0.6239	7.5875	7.6506	0.7576	4.3144	10.47
Hu et al.	0.6235	7.6809	7.7511	0.7357	4.2767	11.13
Ours	**0.7430**	**7.8221**	**7.9341**	**0.8334**	**4.5526**	**5.21**

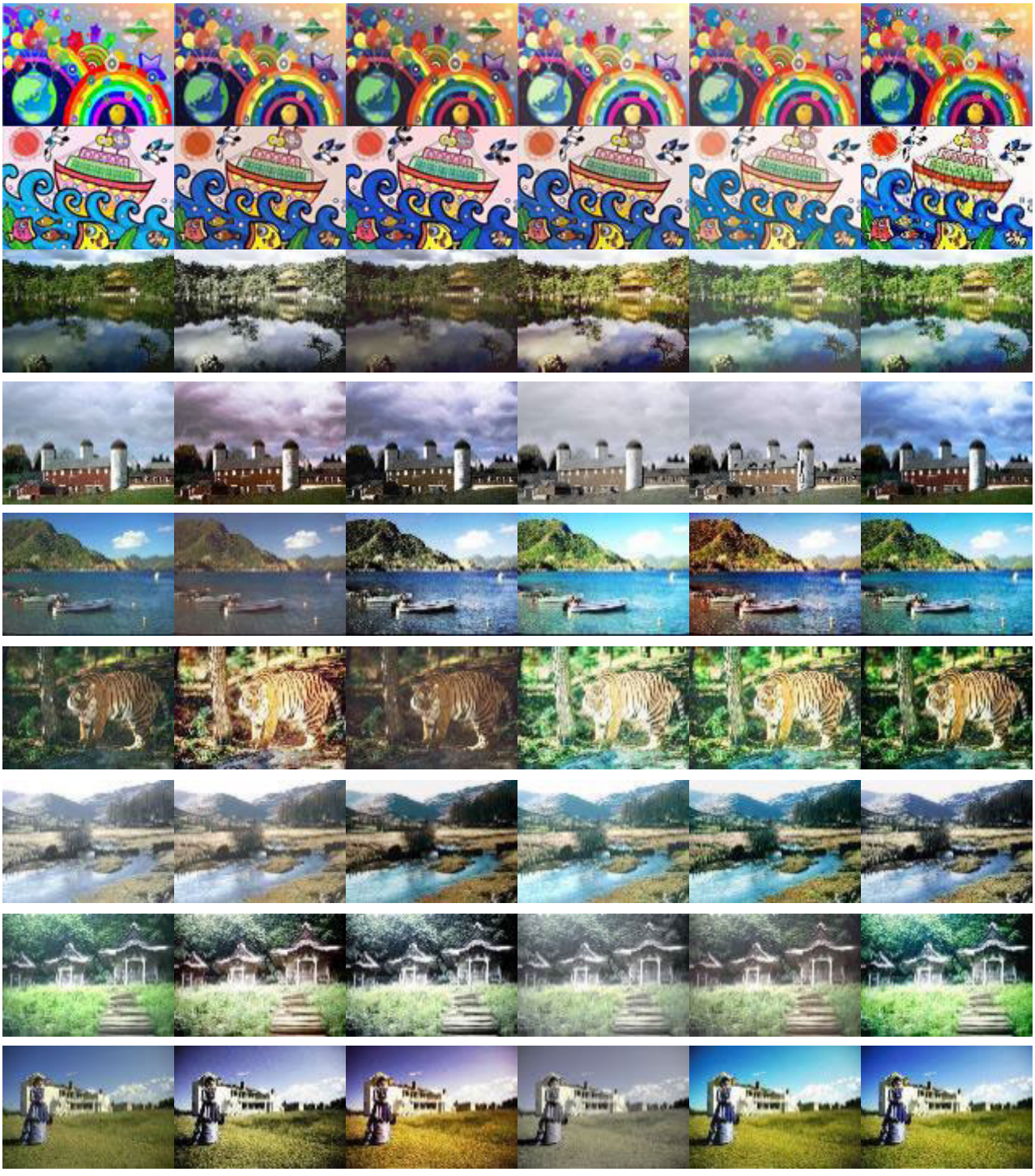

FIGURE 3. Comparing the image effects of different algorithms before and after processing. (a) RGB original images; (b) Du et al.; (c) Braik et al.; (d) Xu et al.; (e) Hu et al.; (f) Ours.

C. ABLATION STUDY

In this section, we will make appropriate changes to the steps of contrast-saturation enhancement in the algorithm to conduct several ablation studies and verify the experimental results of each step. By taking the dreamy rainbow as an example, the comparison of dreamy rainbow images after ablation studies is shown in Fig. 4. The comparison of Fig. 4 (a) and (b) shows that after directly converting RGB to CMY is the problem of blurry image display in addition to narrowing the display color gamut. Although the color contrast

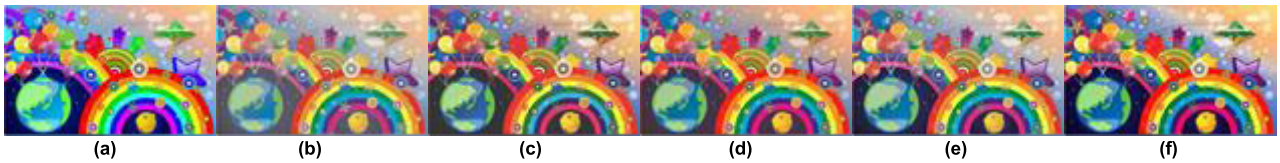

FIGURE 4. Comparison of the image effects before and after using different ablation experiments. (a) RGB original image; (b) directly mapped CMY images; (c) CMY image with contrast enhancement and histogram equalization; (d) CMY image with saturation enhancement; (e) CMY images with error diffusion algorithm; (f) Ours.

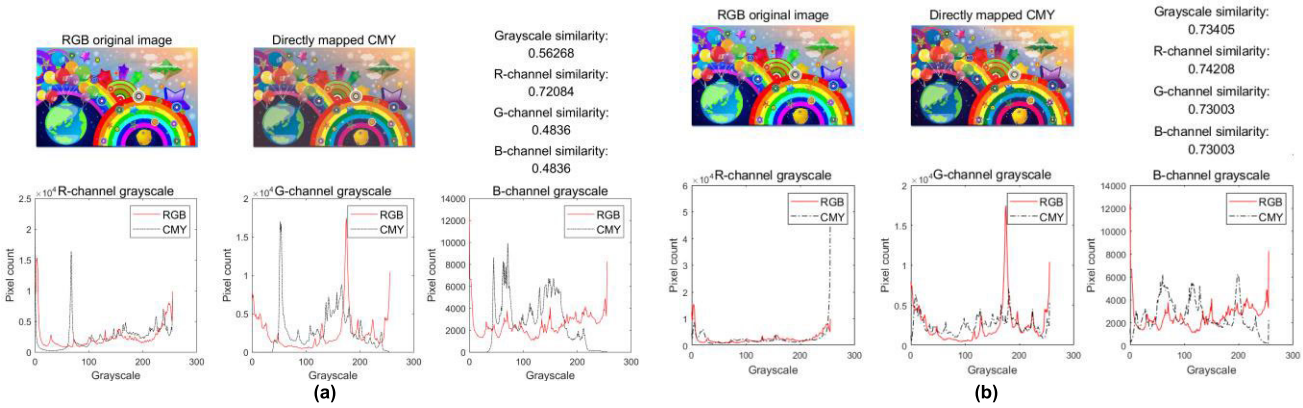

FIGURE 5. Grayscale similarity before and after direct mapping processing and our algorithm processing. (a) CMY directly mapped; (b) our algorithm.

in Fig. 4 (c) has been improved to some extent, there is the problem of being too bright or too dark in some areas. Despite there has been some improvement in color restoration in Fig. 4 (d) (e), the overall effect needs to be further improved. In Fig. 4 (f), The adaptive enhancement algorithm of color conversion in the article takes into account both brightness and color, achieving the conversion of CMY images and color enhancement. In Fig. 5, compared to the original image, we can obtain a comparison of the grayscale similarity (GS) between our algorithm and the direct mapping of the color gamut, as follows:

$$\Delta k = \frac{\sum_{i=1}^{n} \min\left(\mathrm{H}_1(i), \mathrm{H}_2(i)\right)}{\min\left(\sum_{i=1}^{n} \min\left(\mathrm{H}_1(i), \mathrm{H}_2(i)\right)\right)} \tag{13}$$

where $\mathrm{H}_1(i)$,$\mathrm{H}_2(i)$ represents the number of pixels in the i-grayscale level of the image before and after processing, respectively. The RGB three-channel grayscale similarity of the two processed images has significantly improved by our algorithm compared to direct color gamut mapping, with the average grayscale similarity increasing from 0.56268 to 0.73405.

Table 2 shows the various objective evaluation indicators before and after images in the datasets are processed by different ablation studies. As can be seen from the table, it can be seen that the grayscale similarity, information entropy, and structural similarity are higher than those of the direct mapping method, but the signal-to-noise ratio may fluctuate in different ablation studies. Our algorithm is integrated to the characteristics of electrowetting, color conversion, contrast, saturation and other factors. Hence, all evaluation indicators are superior to direct mapping and ablation experiments.

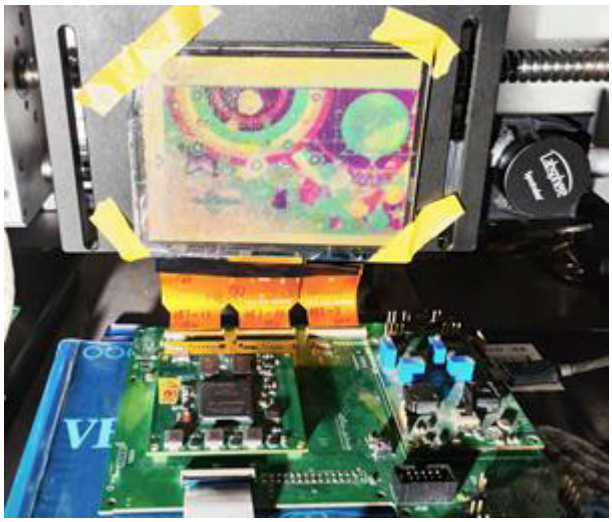

FIGURE 6. The experimental platform of the electrowetting display.

D. EXPERIMENTAL VALIDATION

To verify the feasibility of our algorithm, we also developed a 5.84-inch electrowetting display with CMY three-layer and the relevant driving system. The display has the resolution of 764 × 550, the grayscale of 64 and the pixel density of 161.195 PPI. We fix the chromatic electrowetting screen on the displacement table. The chromatic electrowetting display

FIGURE 7. The display effect of CMY electrowetting electronic paper on images processed by different algorithms under the light source of 5000 K color temperature and 65500 Lux illumination. (a) RGB original images; (b) Du et al.; (c) Braik et al.; (d) Xu et al.; (e) Hu et al.; (f) Ours.

at a 45° angle using a light source with a color temperature of 5000 K and an illumination of 65500 Lux. The electrowetting screen is displayed through the driving system. The experimental platform of the electrowetting display is shown in Fig. 6.

Fig. 7 shows the display effect of CMY electrowetting electronic paper on images processed by different algorithms under a light source with a color temperature of 5000 K and an illumination of 65500 Lux. From the actual display effect of chromatic electrowetting, it can be seen that in some cases where the colors are similar, the contrast of the original image is not high, resulting in color mixing and poor display of details. The overall display effect is darker in low brightness images. In Fig.7(b) (c), the methods of Du et al. and Braik et al. can improve the contrast of images to a certain extent, but the brightness adjustment is not suitable for

TABLE 2. Objective evaluation indicators for images processed by ablation studies.

Method	GS	IE	SNR	SSIM
Directly mapped	0.64873	7.76011	7.52235	0.73318
Contrast enhancement	0.66988	7.68921	7.65271	0.76021
Saturation enhancement	0.62391	7.58752	7.65064	0.75766
Error diffusion	0.62356	7.68096	7.75113	0.73571
Ours	**0.74306**	**7.82212**	**7.93411**	**0.83347**

electrowetting display screens, and sometimes there is a certain color deviation. In Fig.7(d) (e), the methods of Xu et al. and Hu et al. have achieved color conversion and brightness correction to a certain extent, but some bright details in certain scenes have not been further preserved, and sometimes lack a sense of hierarchy between light and dark. In Fig.7(f), the adaptive dynamic enhancement algorithm for color space conversion combined with the diffuse reflection characteristics of electrowetting. Furthermore, the color and image details of electrowetting display are restored through color conversion, contrast-saturation enhancement and brightness correction.

IV. CONCLUSION

The charge capture of pixel electrowetting results in contact angle hysteresis and inconsistent aperture ratio, which narrows the color gamut, merges colors, and reduces contrast of the displayed image. In response to this issue, we propose a dynamic enhanced display with adaptive color conversion based on the aperture ratio of the CMY chromatic electrowetting. In view of the physical characteristics of chromatic electrowetting pixels, we adopt a color conversion method of the aperture ratio allocation, which makes the grayscale distribution of each color channel more reasonable. At the same time, considering the changes of the grayscale mean and aperture ratio with different color electrowetting, we design an adaptive method of dynamic contrast enhancement and segmented histogram equalization based on the change of the aperture ratio. It makes the grayscale of the image more accurate in each stage of ink movement. On this basis, in order to compensate for color loss, we research an adaptive domain error diffusion algorithm under saturation enhancement based on the electrowetting aperture ratio of each color and the different color compression situations. The experimental results demonstrate that compared with other algorithms and ablation research, the objective evaluation of images by our algorithm has been improved to a certain extent, and the overall quality, color, and brightness of images have also been enhanced to a certain extent. Most significantly, the images processed by our algorithm can have better visual display effects on chromatic electrowetting electronic paper, displaying more image information and detailed textures. This is of great significance for optimizing the photoelectric characteristics of electrowetting motion and improving the display performance of electrowetting electronic paper. In future research, I will further combine software and hardware debugging to achieve real-time color conversion and user interaction interface for electrowetting display screens.

ACKNOWLEDGMENT

The authors would like to thank the anonymous reviewer for their valuable suggestions which have greatly improved the manuscript. At the same time, they also would like to thank South China Normal University for providing the chromatic electrowetting display, which helped to successfully complete the experiment.

REFERENCES

[1] S. Lin, Z. Lin, T. Guo, and B. Tang, "Contrast enhancement by intensity preservation-based dynamic histogram equalization for electrowetting display," *IEEJ Trans. Electr. Electron. Eng.*, vol. 15, no. 1, pp. 121–127, Jan. 2020.
[2] B. Cai, C. Tong, Q. Wu, and X. Chen, "Gamma error correction algorithm for phase shift profilometry based on polar angle average," *Measurement*, vol. 217, Aug. 2023, Art. no. 113074.
[3] B. S. Rao, "Dynamic histogram equalization for contrast enhancement for digital images," *Appl. Soft Comput.*, vol. 89, Apr. 2020, Art. no. 106114.
[4] M. Veluchamy and B. Subramani, "Image contrast and color enhancement using adaptive gamma correction and histogram equalization," *Optik*, vol. 183, pp. 329–337, Apr. 2019.
[5] K. Mayathevar, M. Veluchamy, and B. Subramani, "Fuzzy color histogram equalization with weighted distribution for image enhancement," *Optik*, vol. 216, Aug. 2020, Art. no. 164927.
[6] Y. Liu, F. Zhang, Y. Zhang, X. Li, and C. Zhang, "Image smoothing based on histogram equalized content-aware patches and direction-constrained sparse gradients," *Signal Process.*, vol. 183, Jun. 2021, Art. no. 108037.
[7] E. Pashaei and E. Pashaei, "Gaussian quantum arithmetic optimization-based histogram equalization for medical image enhancement," *Multimedia Tools Appl.*, vol. 82, no. 22, pp. 34725–34748, Sep. 2023.
[8] L. Bai, W. Zhang, X. Pan, and C. Zhao, "Underwater image enhancement based on global and local equalization of histogram and dual-image multi-scale fusion," *IEEE Access*, vol. 8, pp. 128973–128990, 2020.
[9] A. Paul, P. Bhattacharya, and S. P. Maity, "Histogram modification in adaptive bi-histogram equalization for contrast enhancement on digital images," *Optik*, vol. 259, Jun. 2022, Art. no. 168899.
[10] B. Subramani and M. Veluchamy, "Quadrant dynamic clipped histogram equalization with gamma correction for color image enhancement," *Color Res. Appl.*, vol. 45, no. 4, pp. 644–655, Aug. 2020.
[11] H. Rahman and G. C. Paul, "Tripartite sub-image histogram equalization for slightly low contrast gray-tone image enhancement," *Pattern Recognit.*, vol. 134, Feb. 2023, Art. no. 109043.
[12] H. Xie, R. Wanat, and M. D. Fairchild, "Perceived color gamut in images: From boundary to difference," *Frontiers Neurosci.*, vol. 16, Jun. 2022, Art. no. 907697.
[13] M. Takeuchi, Y. Sakamoto, R. Yokoyama, H. Sun, Y. Matsuo, and J. Katto, "Gamut-extension methods considering color information restoration," *IEEE Access*, vol. 7, pp. 80146–80158, 2019.
[14] Y. Lu and S.-W. Jung, "Progressive joint low-light enhancement and noise removal for raw images," *IEEE Trans. Image Process.*, vol. 31, pp. 2390–2404, 2022.
[15] S.-C. Pei and C.-T. Shen, "Color enhancement with adaptive illumination estimation for low-backlighted displays," *IEEE Trans. Multimedia*, vol. 19, no. 8, pp. 1956–1961, Aug. 2017.
[16] L. Yu, H. Su, and C. Jung, "Perceptually optimized enhancement of contrast and color in images," *IEEE Access*, vol. 6, pp. 36132–36142, 2018.
[17] T. Azetsu and N. Suetake, "Hue-preserving image enhancement in CIELAB color space considering color gamut," *Opt. Rev.*, vol. 26, no. 2, pp. 283–294, Apr. 2019.
[18] M. Chen, S. Lin, T. Mei, Z. Xie, J. Lin, Z. Lin, T. Guo, and B. Tang, "Research on hydrodynamic characteristics of electronic paper pixels based on electrowetting," *Micromachines*, vol. 14, no. 10, p. 1918, Oct. 2023.
[19] *The Berkeley Segmentation Dataset and Benchmark*. Accessed: Feb. 8, 2021. [Online]. Available: https://www2.eecs.berkeley.edu/Research/Projects/CS/vision/bsds/

[20] *CBSD68-Dataset: Color BSD68 Dataset for Image Denoising Benchmarks*. Accessed: Jul. 26, 2021. [Online]. Available: https://github.com/clausmichele/CBSD68-dataset/
[21] N. Du, Q. Luo, Y. Du, and Y. Zhou, "Color image enhancement: A metaheuristic chimp optimization algorithm," *Neural Process. Lett.*, vol. 54, no. 6, pp. 4769–4808, Dec. 2022.
[22] M. Braik, "Hybrid enhanced whale optimization algorithm for contrast and detail enhancement of color images," *Cluster Comput.*, pp. 1–37, Dec. 2022.
[23] L. Xu, Q. Li, X. Liu, Q. Xu, and M. R. Luo, "Gamut mapping based image enhancement algorithm for color deficiencies," *Biomed. Opt. Exp.*, vol. 12, no. 11, pp. 6882–6896, 2021.
[24] T. Hu, Q. Zhou, X. Nan, and R. Lin, "A color image decomposition model for image enhancement," *Neurocomputing*, vol. 558, Nov. 2023, Art. no. 126772.

MINGZHEN CHEN received the B.S. degree in electronic information science and technology, in 2017, and the M.S. degree in electronic information, in 2020. He is currently pursuing the Ph.D. degree in circuit and system with Fuzhou University, Fuzhou, China. His current research interests include the research of electrowetting display driver and image processing technology.

SHANLING LIN received the Ph.D. degree in electronic circuit and system from the Fuzhou University of China, in 2020. She is currently with the School of Advanced Manufacturing, Fuzhou University. Her main research interests include information display technology, include driving systems for electrowetting display, micro/nano LED, image processing, and other optical information technology.

JIANPU LIN received the Ph.D. degree in physical electronics from Fuzhou University. He is currently a Master Tutor of the School of Advanced Manufacturing, Fuzhou University. He mainly engaged in digital image processing technology, artificial intelligence technology, 3D stereoscopic display technology, new display technology, and other research.

ZHIXIAN LIN received the Ph.D. degree in physical electronics from the Fuzhou University of China, in 2010. From 2007 to 2013, he was an Associate Professor with the Department of Physics and Information Engineering, Fuzhou University, where he has been a Professor with the College of Physics and Information Engineering, since 2013. His research interests include information display technology, printed electronic display, flat panel display device and its drive technology, image processing, and other optical information technology.

TAILIANG GUO received the M.S. degree in applied physics from the Fuzhou University of China, in 1986. From 1995 to 2000, he was a Senior Scholar visited the United States Case Western Reserve University. He has published more than 200 articles on display technologies. His research interests include FED materials and devices, 3D display, printing electronics, and its application.